

Journal Pre-proof

Impact of urban morphology on outdoor air temperature and microclimate optimization strategy base on Pareto optimality in Northeast China

Jun Zhang, Peng Cui, Haihong Song



PII: S0360-1323(20)30415-7

DOI: <https://doi.org/10.1016/j.buildenv.2020.107035>

Reference: BAE 107035

To appear in: *Building and Environment*

Received Date: 5 March 2020

Revised Date: 19 May 2020

Accepted Date: 2 June 2020

Please cite this article as: Zhang J, Cui P, Song H, Impact of urban morphology on outdoor air temperature and microclimate optimization strategy base on Pareto optimality in Northeast China, *Building and Environment* (2020), doi: <https://doi.org/10.1016/j.buildenv.2020.107035>.

This is a PDF file of an article that has undergone enhancements after acceptance, such as the addition of a cover page and metadata, and formatting for readability, but it is not yet the definitive version of record. This version will undergo additional copyediting, typesetting and review before it is published in its final form, but we are providing this version to give early visibility of the article. Please note that, during the production process, errors may be discovered which could affect the content, and all legal disclaimers that apply to the journal pertain.

© 2020 Published by Elsevier Ltd.

1 **Impact of urban morphology on outdoor air temperature and microclimate**
2 **optimization strategy base on Pareto optimality in Northeast China**

3 Jun Zhang^a, Peng Cui^{a,b*}, Haihong Song^a

4 ^a *School of Landscape, Northeast Forestry University, Harbin, 150040, China.*

5 ^b *Heilongjiang Cold Region Architectural Science Key Laboratory, School of*
6 *Architecture, Harbin Institute of Technology, Harbin, 150001, China*

7

8

9

10

11

12

13

14 * Corresponding author:

15 *Associate professor Peng Cui, School of Landscape, Northeast Forestry University,*
16 *Harbin, 150040, China.*

17 *E-mail address: 690471684@qq.com; 14B334004@hit.edu.cn*

18 Tel: 008613351806160. Fax: 0086045186281155

19

20

1 ABSTRACT

2 The urban microclimate is affected by the urban morphology parameters. The
3 objective of this study was to investigate the correlation between air temperature and
4 urban morphology parameters in a cold-climate city in China. Field measurements
5 were performed to record the microclimate parameters at 27 points in a 10 km² urban
6 area in Harbin, China. Multilinear regression models were created to investigate the
7 effects of the urban morphology parameters on the outdoor air temperature. Several
8 interesting findings were obtained. First, the degree of influence of urban morphology
9 on temperature was time-dependent and spatial-dependent, and the largest influence
10 was observed in a 100 m radius around the point of interest. Second, an increase in the
11 green plot ratio of 0.5 decreased (increased) the daytime average temperature by
12 0.8 °C (1.3 °C) in the summer (winter). For the same street width, a 10 m increase in
13 the building height decreased the daytime temperature by 0.06 °C, and for the same
14 building height, a 10 m increase in the street width increased the daytime temperature
15 by 0.17 °C in summer. The daytime average temperature was significantly affected by
16 the number of building floors; however, when the building had more than 20 floors,
17 the temperature did not change significantly with the building height. In addition, a
18 multi-objective optimization framework based on Pareto optimality was used to
19 ascertain the optimal urban morphology layout considering the urban microclimate.
20 The optimal wind and thermal environments were achieved at building densities
21 ranging from 20%-30% and building plot ratios ranging from 3-5.

22

23 *Keywords:* Urban morphology parameters, Urban microclimate, Multi-objective
24 optimality, Northeast China

25

1 Nomenclature

2 *BDG*: Percentage of building area over a surface area

3 *HBDG*: Ratio of the height of building to the percentage of building area

4 *GnPR*: Green plot ratio

5 *LAI*: Leaf area index

6 *PAVE*: Percentage of pavement area (%)

7 *WALL*: Total wall surface area over a 50 m-radius surface area (m^2)

8 *SVF*: Sky view factor

9 *RH*: relative humidity (%)

10 *WIND*: average wind speed (m/s)

11 T_{avg} : Daily average temperature ($^\circ\text{C}$)

12 T_{max} : Daily maximum temperature ($^\circ\text{C}$)

13 T_{min} : Daily minimum temperature ($^\circ\text{C}$)

14 $Ref T_{avg}$: Daily average temperature at a reference point ($^\circ\text{C}$)

15 $Ref T_{max}$: Daily maximum temperature at a reference point ($^\circ\text{C}$)

16 $Ref T_{min}$: Daily minimum temperature at a reference point ($^\circ\text{C}$)

17 *SOLAR*: Daily solar radiation at a reference point (W/m^2)

18

1 **1. Introduction**

2 The urban heat island (UHI) effect is increasing due to increasing urbanization.
3 The urban microclimate is the result of highly dynamic and complex processes that
4 depend on the macroclimate and urban morphology [1]. The microclimate affects
5 human comfort and the utilization of outdoor spaces [2]. Therefore, research on the
6 microclimate of specific cities or sites is required to improve our understanding of the
7 parameters that affect the urban microclimate.

8 The impact of urban morphology on the outdoor microclimate has received
9 significant research interests in recent decades. The temperature inside buildings
10 depends on the proportions of building and vegetation, the building height, wall area,
11 road proportion, and other elements, as well as the regional climate [3,4]. The urban
12 morphology affects the microclimate to varying degrees [5]. Field research by Jusuf
13 and Wong [6] showed that within a 50-m radius, the green plot ratio (GnPR), total leaf
14 area of trees, and the percentage of the green area were critical parameters with
15 significant influences on the minimum temperature and average temperature. The sky
16 view factor (SVF) had a significant influence on the maximum temperature. Field
17 research in Beijing by Yan [7] indicated that urban morphology had the most
18 significant impact on the temperature within a 75-m radius, and this range was the
19 same as that in Tokyo [8]. The urban geometry and the thermal properties of urban
20 surfaces were also important parameters influencing the microclimate [9]. Land cover
21 features, such as the ratio of building to vegetated areas, affect the microclimate. The
22 SVF, which depends on the site geometry, is another crucial factor affecting the mean
23 radiant temperature [10]. However, some studies have shown that the SVF had a
24 negligible impact on air temperature [11,12]. The air temperature is correlated with

1 the green ratio and the building ratio and depends on the time of year (day) and the
2 weather [13-15]. The parameters that affect the outdoor microclimate and the radius
3 of influence in cold cities such as Harbin remain unclear.

4 Empirical models that describe the relationship between urban morphology
5 parameters and microclimate parameters based on field measurements are commonly
6 used to assess the influence mechanism of urban morphology on the microclimate.
7 Kruger and Givoni [16] developed equations to correlate the maximum, minimum,
8 and average air temperatures with the water area, built area, open area, paved area,
9 and green area in Curitiba. The equations were used to predict the temperature of
10 areas with the same urban morphology. Tong [17] applied the same method in Tianjin,
11 China and found that an increase in the number of building levels and reduction in
12 pavement width lowered the T_{max} and $T_{avg-day}$ and increase the T_{avg} , T_{min} , $T_{avg-night}$.
13 Moreover, an increase in the $GnPR$ of 0.5 lowered the T_{min} and $T_{avg-night}$ by 0.7 °C and
14 0.5 °C respectively.

15 Outdoor microclimate optimization should consider the influence mechanism of
16 urban morphology on each climate factor. The optimization of a single goal may
17 adversely affect other goals. Therefore, the comprehensive optimization of multiple
18 microclimatic factors is of practical significance to improve the urban environment.
19 We use the strength Pareto evolutionary algorithm (SPEA-2) [18] to develop design-
20 based recommendations. Schaffer [19] proposed the multi-objective vector evaluated
21 genetic algorithm (VEGA) algorithm in 1985. Subsequently, Goldberg and Pareto
22 [20] proposed the Pareto frontier theory to calculate the optimal solution set. SPEA-2
23 is the revision of a previously developed algorithm and provides improved accuracy
24 of the optimal solution [21]. Previous researchers have used genetic algorithms for the

1 optimization of the energy balance of the building environment and traffic
2 optimization. However, few studies have considered wind speed, sunshine duration,
3 and temperature as optimization objectives to develop urban design-based
4 recommendations.

5 The objective of this study is to investigate the effects of urban morphology on
6 temperature and use the SPEA-2 algorithm to develop an urban morphology
7 optimization strategy to improve the thermal environment. Meteorological data were
8 obtained in the field to investigate the spatial and temporal microclimate parameters
9 in Harbin. The influence of the urban morphology parameters on the air temperature
10 and the radius of influence of the urban morphology parameters were analyzed. A
11 multi-objective optimization framework was used to determine the optimal urban
12 morphology considering the urban microclimate, and design-based recommendations
13 were presented for the early stage of urban design.

14 **2. Methodology**

15 *2.1. Study area*

16 Harbin ($125^{\circ} 42' - 130^{\circ} 44'E$ longitude, $10^{\circ} 04' - 46^{\circ} 40'N$ latitude) is the
17 capital of Heilongjiang province and the largest city in northeastern China. The area
18 has a temperature continental monsoon climate with long winters and short summers
19 [22]. The annual average precipitation is 569.1 mm, and the snow period is from
20 November to January. The T_{avg} is $-19^{\circ}C$ in winter and $23^{\circ}C$ in summer. The study
21 area is 10.1 km^2 , with a perimeter of 6.5 km and includes pedestrian streets, plazas,
22 and small parks. The urban area has an open block layout. The study area is
23 characterized by high building density, moderate vegetation cover, multi-story and

1 high-rise buildings, and diverse block types; the morphological characteristics and
2 functional types are those of open blocks. The layout of the study area is shown in
3 Fig. 1.

4 **Insert Fig. 1**

5 *2.2. Microclimate parameter measurements*

6 The outdoor microclimate was assessed using 27 measuring points arranged in a
7 grid with a distance of 100-200 m, as shown in Fig. 1. Most of the block morphology
8 in the area was covered by the measuring points. The microclimate parameters that
9 were measured included air temperature, relative humidity, and wind speed. The
10 microclimate station is shown in Fig. 2, and the sensor precision is listed in Table 1.
11 Measurements were obtained automatically and synchronously at each location every
12 5 min. The sensors were wrapped in aluminum foil, leaving a gap in the middle to
13 minimize the influence of solar radiation on the temperature. The weather stations
14 were placed at the height of 1.5 m on a tripod to obtain data at the height of
15 pedestrians.

16 **Insert Fig. 2**

17 **Insert Table 1**

18 The focus of this study was to determine the impact of urban morphology on air
19 temperature during summer and winter; therefore, fairly clear, calm, and sunny
20 weather conditions were preferred so that the data represented typical winter or
21 summer weather conditions [23]. According to the Harbin observatory, the T_{avg} should
22 be above 25 °C in summer and below -7 °C in winter to represent typical summer and
23 winter meteorological conditions. The average wind speed in an urban area should be

1 lower than 3 m/s at the height of a pedestrian. Therefore, the days chosen for the
2 analysis in this study had to match the following conditions:

- 3 ■ The maximum solar radiation had to be higher than 800 W/m^2 in summer and
4 lower than 900 W/m^2 in winter;
- 5 ■ The hourly solar radiation and air temperature profiles had to be normally
6 distributed;
- 7 ■ The daily air temperature had to be higher than 25°C in summer and lower than -
8 7°C in winter;
- 9 ■ The daily average wind speed had to be less than 3 m/s, and there should be no
10 rain or snow.

11 The measuring points were located in open areas of the block. Since several
12 researchers were required to monitor the sensors, continuous daily monitoring was not
13 possible. Therefore, we selected 40 d during Dec. 2017 to Aug. 2018 that met the
14 conditions, and the plan was confirmed based on the weather forecast. Some
15 modifications were made due to wrong weather forecasts and instrument failure; we
16 eventually selected 35 d and randomly divided them into two groups used for model
17 development (30 d) and validation (5 d), respectively (Table 2). The measurements
18 were conducted from 0:00 to 24:00 continuously on each day.

19 **Insert Table 2**

20 *2.3. Urban morphology parameters measurement and computation*

21 Geographic Information System (GIS) mapping is an effective method to link the
22 urban morphology parameters with the local microclimate [24]. Urban planning is

1 influenced by history and culture, and urban morphology has individual
2 characteristics [25]. In reference to international studies, the following four criteria
3 should be met in the selection of urban morphology parameters:

- 4 1. The parameters should significantly affect the microclimate
 - 5 2. The parameters should be easy to extract and calculate
 - 6 3. The parameters affect the design
 - 7 4. Parameter redundancy should be avoided

Several parameters were chosen in this study. The *GnPR* affects the regional temperature by reducing heat loss through evaporation. The *SVF* affects solar radiation. The *HBDG* affects the solar heat gain resulting from solar radiation. The *WALL* affects the indoor and outdoor heat exchange, and the *PAVE* affects ground surface heat exchange. A quantitative GIS analysis of the parameters was conducted to determine the influence of the urban morphology parameters on the temperature.

As shown in Fig. 3a, the measurement points are located in different land cover classes, resulting in differences in the temperature range. Therefore, the morphology of the points was quantified after establishing buffer zones with radii of 20 m, 50 m, 100 m, and 150 m, as shown in Fig. 3b.

Insert Fig. 3

19 The values of *PAVE*, *HBDG*, and *WALL* were extracted from the GIS data. We
20 used an 8-mm circular fisheye lens to obtain images that were imported into the
21 Rayman model to obtain the *SVF* values [26]. For the *GnPR* calculation, we used the
22 following equation [27]:

$$GnPR = \sum (n_m A_m \times LAI_m) / Site\ Area \quad (1)$$

where LAI_m is leaf area index of species m , A_m is canopy area of species m , n is the number of plants of species m on the site. The morphology information of each test point was shown in Table 3.

Insert Table 3

6 2.4. Regression analysis and model development

7 Multiple regression analysis was conducted using the following steps:

Step 1: We obtained the microclimate data at the measurement points, including air temperature, wind speed (*WIND*), and relative humidity (*RH*). We calculated the morphology parameters of the measurement points in the 20 m, 50 m, and 100 m buffer zone using the GIS data.

Step 2: We established regression models to describe the relationship between the air temperature and the morphology parameters. The air temperature was the dependent variable, and the reference microclimate data (*Ref T, SOLAR*) were obtained from the observatory, the measured data (*WIND, RH*), and the morphology parameters were the independent variables. The regression model is defined as:

$$T = a + b_1 RefT + b_2 SOLAR + b_3 WIND + b_4 RH + b_5 HBDG + b_6 GnPR + b_7 SVF + b_8 PAVE + b_9 WALL \quad (2)$$

19 where a is the constant, b_n is regression coefficient, and other variables can refer to
20 Nomenclature part. The model was built based on integrated outdoor temperature, so
21 for dependent variables, T include the T_{avg} , T_{max} , T_{min} , and independent variables, Ref
22 T was the corresponding reference average, maximum, minimum temperature.

1 Step 3: The results were calculated in the different buffer zones. We established
2 quantitative relationships for one-to-one correspondences to determine the degree of
3 influence of the factors in the range.

4 Step 4: We calculated the Pearson correlation coefficient (r), the coefficient of
5 determination (R^2), and the significance (p -value) of the independent variables. If the
6 R^2 was larger than 0.7 and the p -value denoted by *Sig.* (2-tailed) was smaller than
7 0.05, the variable was used in the final equation. The strength of the linear
8 relationship was evaluated. If the R^2 between two independent variables was larger
9 than 0.7, the variables were considered to be self-dependent and were excluded from
10 the equations. The R^2 of the equations for the different buffer zone were compared,
11 and the equation with the largest R^2 was used as the final model.

12 *2.5. Multi-objective optimization model*

13 Each urban morphology parameter has a different influence on each
14 microclimate parameter. For example, an increase in the street height to width (H/W)
15 ratio can lower the air temperature and solar radiation and increase the wind speed,
16 resulting in a comfortable thermal environment but an uncomfortable wind
17 environment. In addition, a morphology that provides a comfortable thermal
18 environment in the summer may result in an uncomfortable environment in the winter.
19 In these cases, a multi-objective optimization using the Pareto optimal solution set is
20 suitable [20].

21 The evaluation criteria for this solution are as follows: If the output performance
22 is balanced when all optimization objectives are considered, the performance
23 improvement of one optimization objective is greater than or equal to that of another

1 optimization objective. The solution set with a balanced performance is called the
 2 non-dominant solution set. The solution set with the best equilibrium performance is
 3 called the optimal solution set. The non-dominant solution set distribution is called
 4 the Pareto frontier. The ultimate goal of multi-objective optimization is to obtain the
 5 Pareto frontier solution set. The mathematical definition of multi-objective
 6 optimization is as follows:

$$\begin{aligned} 7 \quad & \min f(x) = [f_1(x), f_2(x), \dots, f_p(x)]^T, \\ 8 \quad & g_i(x) \geq 0, i \in I, \\ 9 \quad & h_j(x) = 0, j \in E \end{aligned} \tag{3}$$

10 where for multi-objective programming (MOP), the variable feasible region is S , and
 11 the target feasible region is $Z=f(S)$. For a viable solution $x^* \in S$, solution should be
 12 $\forall x \in S, f(x^*) \leq f(x)$; therefore, x^* is the optimal solution for multi-objective
 13 optimization. If $x \in S$ does not exist, then $f(x) < f(x^*)$, where x^* is called the efficient
 14 solution or the Pareto optimal solution of MOP.

15 After determining the influence of the urban morphology of Harbin on the
 16 microclimate, we conducted a sensitivity analysis, simplified the parameters, and used
 17 Grasshopper plug-in [28] of the Rhino modeling software to conduct parametric
 18 modelling of the urban morphology. For the microclimate simulation, the Radiation
 19 software was used to calculate the solar radiation and the sunshine duration, the
 20 Ladybug software was used to calculate the temperature using the proposed equations,
 21 and the Butterfly software was used to calculate the wind speed. For the multi-
 22 objective optimization, Octopus software was used to calculate the optimal solution

1 set according to the simulation data. All the software modules were integrated using
2 Grasshopper plug-in.

3 Many urban morphology indicators influence the accuracy of the optimization
4 result, such as *BDG* and *HBDG*. Therefore, the complex urban morphology
5 parameters were simplified into basic morphological variables as building height,
6 building row spacing, column spacing, and building layout to guide the urban design.
7 We then used the optimal solution set and calculated the *BDG*, *PAVE*, *HBDG*, and
8 other urban design indicators using the basic morphological variables. The
9 optimization logic is shown in Fig. 4.

10 **Insert Fig. 4**

11 The basic situation of the urban block layout was investigated in Harbin. The
12 constraints for the model establishment and the simplification of the urban
13 morphology parameters were as follows based on the field survey.

14 Site area: the basic block unit is 400 m×400 m, the road width is 15 m-25 m,
15 and the building height is 0-150 m, where 0 indicates an open space. The block gap
16 rate is an essential factor determining the thermal environment and wind environment.
17 The row spacing and column spacing are the only factors that determine the gap rate.
18 According to the field survey, we simplified the conditions at the simulation site as 3-
19 5 columns and 3-5 rows. The column separation distance was > 1.8 times the building
20 height and < 50 m, according to the city planning department needs. The minimum
21 building area should be > 750 m² and < 5000 m². The mathematical expressions are as
22 follows:

$$\begin{aligned}
 & \left\{ \begin{array}{l} 0 \leq H \leq 150 \\ 50 \geq D_1 \geq 1.8H \\ 50 \geq D_2 \geq 6 \\ L = \frac{400 - (a-1)D_1}{a} (3 \leq a \leq 5) \\ W = \frac{400 - (b-1)D_2}{b} (3 \leq b \leq 5) \\ 5000 \geq L * W \geq 750 \end{array} \right. \quad (4)
 \end{aligned}$$

where H is the building height, D_1 is the building row spacing, D_2 is the column spacing, L is the building length, W is the building width, a is the number of rows, and b is the number of columns. The Grasshopper software can generate all possible layouts of the buildings using these equations.

A previous study on human thermal comfort in Harbin indicated that the summer outdoor microclimate is comfortable for tourists. However, in the winter, solar radiation and wind speed are the primary factors causing discomfort for tourists [29]. Therefore, in this study, the optimization objectives were to increase the sunshine duration in the winter, increase the heat gain of the site, and reduce the overall wind speed.

Optimization target for solar radiation: the objective was to increase the average sunshine hours. We selected the average sunshine hours (h) on the south facade of the building on a cold day at 1.5 m. The optimization objective function is $\alpha=1/h$.

Optimization target for the thermal environment: the objective was to increase the maximum heat gain of the site. The average solar radiation of the site in winter is I , and the optimization objective function is $\gamma=I$.

Optimization target for the wind environment: the objective was to reduce the average wind speed (V_{avg}), and the optimization objective function is $\beta=1/V_{avg}$.

1 **3. Results and analysis**

2 *3.1. Influence of temporal and spatial variation on the microclimate*

3 Figure 5 shows the temperature mapping at the different measuring points during
4 the daytime (14:00) and nighttime (2:00) in summer. Figure 6 shows the temperature
5 mapping during the daytime (14:00) and nighttime (2:00) in winter.

6 **Insert Fig. 5**

7 *a. Daytime temperature distribution in the summer.* As Fig. 5a shows, the
8 temperatures were significantly different at the different locations, even in a small
9 area, due to the differences in *HBDG*, *SVF*, *GnPR*, and *PAVE* at each measuring point.
10 The highest temperature difference was 3.88 °C. The highest temperature of 29.19 °C
11 occurred at measuring points 5. The lowest temperature was 25.31 °C at measuring
12 points 13 and 14. The temperatures at measuring points 5, 16, and 17 in the square
13 were significantly higher than those of the other measuring points during the day. The
14 reason is the absence of shelter in the square, resulting in heat absorption. The lowest
15 temperature occurred in the park, where the dense vegetation reduced the temperature.
16 It is worth noting that the temperature of the measuring point in the central street was
17 significantly lower than that in the surrounding area; this result was attributed to the
18 lack of vehicles in the pedestrian area and the dense landscape trees on both sides of
19 the streets that block the sunshine, resulting in relatively low temperatures.

20 *b. Nighttime temperature distribution in the summer.* As Fig. 5b shows, the
21 maximum temperature difference was 2.37 °C; the highest temperatures occurred at
22 points 22 and 23 (19.19 °C), and the lowest temperature was observed at point 13
23 (16.82 °C). The temperatures at measuring points 5, 16, and 17 in the square were

1 significantly lower than the points in the surrounding area, which was due to the high
2 SVF and rapid heat dissipation at night. The temperatures of the measuring points near
3 the park were significantly lower than those of the other areas, showing heat
4 diffusion. A "cool island effect" occurred in the dense trees, which reduced the
5 surrounding temperature.

6 **Insert Fig. 6**

7 *a. Daytime temperature distribution in the winter.* As Fig. 6a shows, the
8 maximum difference in the daytime temperature (1.5°C) was lower in winter than in
9 summer. The highest temperature (-19.2°C) was observed at point 3, and the lowest
10 temperature (-20.7°C) occurred at point 14. The temperatures at points 5, 16, and 20
11 were significantly higher than those of the other points in the surrounding area.
12 However, the temperatures of points 13 and 14 in the park were lower than those of
13 the other areas, although the leaf area index (*LAI*) index is low in the winter. The low
14 temperatures in the area are attributed to the lack of indirect radiation from the
15 buildings, the tree branches that block solar radiation, and the snow covering large
16 areas.

17 *b Nighttime temperature distribution in the winter.* As Fig. 6b shows, the
18 maximum nighttime temperature difference during winter was 5.1°C . The highest
19 temperature was -22.8°C in the area near point 18, and the lowest temperature was -
20 28°C at point 9. The trends of the daytime and nighttime temperatures exhibited
21 opposite trends. The reason is that in the winter, there is no green vegetation, and solar
22 radiation is the main factor influencing the air temperature. The *SVF* affects the
23 outdoor heat gain, and the *GnPR* and *HBDG* affect the heat loss in the region,

1 resulting in the different trends of the daytime and nighttime temperatures.

2 Different fluctuations in the temperature were observed in the two seasons. As
3 Fig. 7 shows, the degree of influence of the urban morphology on the temperature
4 depended on the season. In the summer, the temperature differences were in the range
5 of 2.6-4.68 °C during the day and 1.75-2.37 °C during the night. In the winter, the
6 range was 2.45-3.6 °C during the day and 3.33-4.6 °C during the night. The ranking of
7 the temperature range in the two seasons, which reflects the degree of influence of
8 urban morphology on the temperature, was summer daytime temperature > winter
9 nighttime temperature ≈ winter daytime temperature > summer nighttime temperature.
10 The ranking of the maximum temperature difference was summer daytime
11 temperature (4.68 °C) > winter nighttime temperature (4.6 °C) > winter daytime
12 temperature (3.6 °C) > summer nighttime temperature (2.37 °C).

13 **Insert Fig. 7**

14 *3.2. Correlation between air temperature and urban morphology parameters*

15 The proposed empirical model was based on the comprehensive outdoor
16 temperature [30]. The empirical prediction model used the T_{min} , T_{avg} , and T_{max} to
17 predict the daytime, nighttime, and average temperatures. Table 4 shows the
18 correlation coefficient between the urban morphology parameters and the temperature
19 in the different buffer zones. The morphology parameters had the highest correlation
20 with the temperature in the buffer with the 100 m radius; therefore, 100 m was
21 selected as the radius in the model.

22 **Insert Table 4**

23 Table 5 shows the relationship between the morphological parameters and the

1 temperature change and the results of the sensitivity analysis. Not all the parameters
2 had an effect on the temperature. The *RH* and *SVF* were not significantly correlated
3 with T_{min} in winter and summer. The *RH* was not significantly correlated with T_{avg} in
4 winter. The *RH* and *GnPR* were not significantly correlated with T_{max} in winter and
5 summer. *WIND* was not significantly correlated with T_{max} in winter.

6 **Insert Table 5**

7 We divided the reference temperature into temperatures higher and lower than
8 0 °C so that the model is widely applicable. Table 6 shows the multiple regression
9 results of the relationship between the air temperature and urban morphology
10 parameters.

11 **Insert Table 6**

12 When the temperature is above 0 °C, 97% of the variation of T_{avg} is explained by
13 the morphological factors. The *SVF* has the largest influence; a 10% increase in the
14 *SVF* increases the T_{avg} by 0.81 °C. For every 10% increase in the *GnPR* (*HBDG*), the
15 T_{avg} decreases by 0.04 °C (0.02 °C). For every 10% increase in *PAVE* and every 10000
16 m^2 increase in the *WALL*, the T_{avg} increases by 0.01 °C and 0.21 °C, respectively; 96%
17 of the variation of the T_{max} and 96% of the variation of T_{min} are explained by the
18 morphological parameters.

19 When the temperature is below 0 °C, 95% of the variation of T_{avg} is explained by
20 the morphological factors. The *SVF* has the largest influence; a 10% increase in the
21 *SVF* results in an increase in the T_{avg} of 1.32 °C. For every 10% increase in the *GnPR*
22 (*PAVE*), the T_{avg} increases by 0.06 °C (0.007 °C). For every 10% increase in *HBDG*
23 and every 10000 m^2 increase in the *WALL*, the T_{avg} increases by 0.1 °C and 0.23 °C,

1 respectively; 91% of the variation of the T_{max} and 90% of the variation of T_{min} are
2 explained by the morphological parameters.

3 The standard root mean square error (NRMSE) was used to evaluate the results.
4 Five days of the measurement data (see Table 2) were used as the verification
5 reference.

$$6 \quad NRMSE = \frac{RMSE_i}{RMSE_{i=ref}} = \sqrt{\frac{\sum_1^{Nd} \sum_1^{Ns} (T_{mea,i}(j) - T_{est,i}(j))^2}{\sum_1^{Nd} \sum_1^{Ns} (T_{mea,i}(j) - T_{ref,i})^2}} \quad (5)$$

7 where $NRMSE$ represents the standard root mean square error; $RMSE_i$ stands for the
8 forecast temperature calculated by the equation in Table 6; $RMSE_{i=ref}$ is the reference
9 temperature; $T_{mea,I}(j)$ is the measured temperature at point j on day I . The range of I is
10 1,2... Nd ; Nd represents the number of days used for verification, it is 5 this time. The
11 range of j is 1,2... Ns ; Ns is the number of measurement points used for verification, it
12 is 27 this time; $T_{est,I}(j)$ is the predicted temperature of measuring point j on day I ; $T_{ref,I}$
13 is the reference temperature of the city on day I . The error analysis results are shown
14 in Fig. 8.

15

Insert Fig. 8

16 *a. The reference temperature is above 0 °C:* As Fig. 8a shows, the error range
17 within ± 1 °C accounts for 96% of the prediction results (the light gray part in the
18 figure), and the error range within ± 0.5 °C accounts for 54% of the prediction results
19 (the dark gray part in the figure).

20 *b. The reference temperature is below 0 °C:* As Fig. 8b shows, the error range
21 within ± 1 °C accounts for 85% of the prediction results (the light gray part), and the
22 error range within ± 0.5 °C accounts for 41% of the prediction results (the dark gray

1 part).

2 *3.3. Multi-objective optimization of microclimate*

3 The calculation took 180 hr, and 42 generations and 5368 cases of the layout
4 were calculated. The convergence occurred in the 30th generation, and the
5 convergence correlation coefficient was 0.99. A total of 75 cases were obtained after
6 convergence. The calculation results are shown in Fig. 9.

7 **Insert Fig. 9**

8 *a. The optimal solution sets in different generations.* As Fig. 9a shows, the
9 number of the optimal solution set decreases with an increase in the optimization
10 generation and stabilizes after convergence (30th generation), the final optimal
11 solution set were 75 cases.

12 *b. Schematic diagram of multi-axis space.* As Fig. 9b shows, the sunshine
13 duration, solar radiation, and wind speed influence each other (the closer the distance
14 is to the origin of the coordinate axis, the better the results meet the optimization
15 goal). Therefore, the proposed threshold is important. The black curve shows the
16 change in the optimal solution set. The curves of the three parameters are located in
17 the middle region (middle of the coordinate axis). The optimization result shows that
18 the performance was best for the wind speed optimization (closest to the origin of the
19 coordinate axis).

20 *c. Spatial distribution of Delaunay grids. d. Pareto frontier distribution map.* As
21 Fig. 9c and d shows, the final results were all located on the Pareto frontier, and the
22 red point in the figure is the optimal solution set.

23 The influence of the morphological parameters on the microclimate can be

1 determined by normalizing the difference between the optimization objective and the
2 control variables of the simulation results. The results are shown in Fig.10.

3 **Insert Fig. 10**

4 *a. Optimal target value.* As Fig. 10a shows, the optimization logic of the target
5 was as follows: the optimization process starts by determining the sunshine duration
6 and wind speed that result in the optimal temperature (the radiation temperature
7 variance is the minimum). The wind speed is increased gradually to obtain the
8 minimum wind speed difference. The maximum sunshine duration was determined
9 based on the sunshine duration range. The solution conforming to the Pareto frontier
10 is selected as part of the optimal solution set.

11 *b. Morphology parameters value.* As Fig. 10b shows, the following trends of the
12 morphology parameters were observed. The building height increased, and the
13 number of rows and columns decreased. The distance between the front and back
14 buildings increased, and the distance between the left and right buildings decreased.

15 As shown in Table 7, as the number of generations increases, the building height
16 and spacing gradually increase from south to north. The sunshine duration in the
17 streets increased significantly (the blue color indicates insufficient sunshine duration),
18 and the high-rise building areas meet the requirements for the sunshine duration. By
19 the 30th generation, the optimum sunshine duration was obtained. The temperature
20 changes in the block are balanced, and the wind speed also decreased significantly
21 (the areas in red have higher wind pressure; the large the number of areas in red, the
22 lower the wind speed is).

23 **Insert Table 7**

1 Due to a change in the optimization logic, in the initial generations, the building
2 spacing and height changed based on the standard layout. In the middle of the
3 optimization process, the individual building area and the height changed. After the
4 convergence, the building density and block use efficiency were higher than before
5 the convergence; however, the building height increased to meet the requirements of
6 the sunshine duration and wind speed. Therefore, by considering the quantitative
7 relationship between the calculated values (building height, number of buildings in
8 the plot, number of buildings in the columns, and building spacing) and the mean
9 value of the optimization target (sunshine hours, wind speed, solar radiation), a
10 suitable optimization strategy of the urban microclimate can be determined.

11 **4. Discussion and urban design recommendations**

12 *4.1. Parametric study*

13 A parametric study was conducted to develop design recommendations on the
14 street scale. Our results showed that the morphological parameters that affected the
15 outdoor temperature were *HBDG*, *SVF*, *GnPR*, and *PAVE*, which were simplified into
16 building height, street width, and vegetation area. The height of the building and the
17 street width influenced the *SVF*, *HBDG*, and *PAVE*. The calculated parameters of the
18 simplified model are shown in Table 8.

19 **Insert Table 8**

20 Figure 11 shows the calculation results of the street layout of Model 1 in the
21 summer. As Fig. 11a shows, the T_{max} of all street widths decreases with an increase in
22 the building height. For every 10 m increase in the building height, T_{max} decreases by
23 0.06 °C. At the same building height, for every 10 m increase in the street width, T_{max}

1 increases by 0.17 °C.

2 As Fig. 11b shows, T_{min} of all street widths increases with the height of the
3 buildings. T_{min} increases by 0.07 °C, on average, for every 10 m increase in building
4 height. The street width has no significant influence on the temperature. In the high-
5 rise areas, a 10 m increase in the street width results in an increase in the temperature
6 of 0.01 °C.

7 As Fig. 11c shows, T_{avg} varies significantly in the building area with 2-20 floors;
8 however, when the building has more than 20 floors, the temperature does not change
9 significantly. The temperature of the narrow streets is significantly higher than that of
10 the wide streets for the same building height. For buildings exceeding 30 floors (90
11 m), the street width has no effect on the T_{avg} .

12 Insert Fig. 11

13 Figure 12 shows the calculation results of the street layout of Model 1 in the
14 winter. As Fig. 12a shows, for building with 2-20 floors, T_{avg} increases significantly
15 with an increase in the number of floors. For buildings with less than 20 floors, the
16 change in the street width has a negligible influence on the temperature; For buildings
17 with more than 20 floors, the temperature is higher for narrow streets, and the
18 temperature decreases by 0.05 °C for every 10 m increase in the street width.

19 As Fig. 12b shows, T_{min} increases by 1.3 °C for an increase in 10 floors (30 m)
20 for all street widths. For buildings with less than 20 floors and street widths of 25 m,
21 35 m, and 45 m, the change in T_{min} is relatively small. For buildings with more than
22 20 floors, T_{min} decreases by 0.2 °C for every 10 m increase in the street width.

1

Insert Fig. 12

2 Figure 13 shows the results of the street layout of Model 2. As Fig. 13a shows,
3 T_{avg} has a linear relationship with the number of building floors in the summer as a
4 result of the influence of $GnPR$. T_{avg} decreases by 0.5 °C for every 0.5 increase in the
5 $GnPR$. A 0.5 increase in the $GnPR$ results in a decrease in T_{min} of 0.8 °C (Fig. 13b). As
6 Fig. 13c shows, for the same $GnPR$, T_{min} decreases by 0.3 °C for an increase in 10 m
7 of the building height in the winter. At the same building height, T_{min} increases by
8 1.3 °C for every 0.5 increase in the $GnPR$.

9 Therefore, the $GnPR$ should be increased on both sides of the street, and the
10 height of the buildings should be minimized to achieve heating up in winter and
11 cooling down in summer.

12

Insert Fig. 13

13 *4.2. Urban design recommendations*

14 This section focuses on the urban design recommendations at the block scale. Of
15 the 5,368 cases calculated in this study, the solution set for the microclimate
16 optimization contains 75 optimal layouts. The optimal solution set does not provide a
17 single index but rather a comprehensive index. The overall comfort of the people in a
18 block should be comprehensively evaluated by using a block planning index, namely
19 the BDG and $HBDG$.

20 Figure 14 shows the results of the correlation analysis between BDG and the
21 proportions of the wind and thermal comfort zones. As shown in Table 7, the comfort
22 zone for solar radiation is the orange and red area; the comfort zone for the wind
23 speed is defined as the percentage of the area in red and orange in the whole area.

1

Insert Fig. 14

2 As Fig. 14a shows, *BDG* is negatively correlated with the proportion of thermal
3 comfort zone ($R^2=0.57$), indicating that the area of the thermal comfort zone decreases
4 as the building density increases.

5 Figure 14b shows a significant positive correlation between the *BDG* and the
6 proportion of the comfort zone for wind speed ($R^2=0.88$). This result demonstrates
7 that the area of the wind comfort zone increases significantly as *BDG* increases. The
8 relationship between *BDG* and the wind speed and solar radiation is the opposite.
9 Therefore, there is a range where the comfort zones for both the wind speed and solar
10 radiation coincide. Finding a compromise set of two fitted curves, the range for *BDG*
11 is 20%-30%.

12

Insert Fig. 15

13 Figure. 15 shows the results of the correlation analysis between *HBDG* and the
14 proportions of the wind speed and thermal comfort zones. As Fig. 15a shows, *HBDG*
15 is negatively correlated with the proportion of thermal comfort zone ($R^2=0.66$). This
16 R^2 value is higher than that of *BDG*. It is worth noting that the overall dispersion
17 degree in the fitting diagram is low, and only two points have high dispersion degrees.
18 The R^2 is 0.85 if these cases are excluded, indicating that the primary factor
19 influencing the proportion of the thermal comfort zone is the *HBDG*.

20 As Fig. 15b shows, *HBDG* is positively correlated with the proportion of the
21 wind speed comfort zone ($R^2=0.64$). An increase in *HBDG* significantly reduces the
22 wind speed in the winter and increases the proportion of the wind speed comfort zone.
23 Since the wind speed and thermal comfort zones in the block are relatively balanced,

1 when finding a compromise set of two fitted curves, the *HBDG* should range from 3
2 to 5.

3 **5. Conclusions**

4 In this study, empirical models were developed to predict spatial and temporal
5 changes in the air temperature at the street scale. A parametric study was conducted to
6 assess the impact of urban morphology on the air temperature in summer and winter.
7 It was found that an increase in the number of building levels and a reduction in the
8 street width in the summer reduced T_{max} and T_{avg} and increased T_{min} . An increase in
9 the *GnPR* of 0.5 decreased the T_{avg} and T_{min} by 0.5 °C and 0.8 °C, respectively in the
10 summer. In the winter, the temperature change is influenced by the number of
11 building floors on both sides of the street. When the building floors are below 20, an
12 increase in the building height and street width of 10 m, T_{avg} increases 0.03 °C and
13 decreases 0.05 °C respectively. When the building floors are above 20, an increase in
14 the building height and street width of 10 m, T_{min} increases by 0.4 °C and decreases by
15 0.05 °C respectively. At the same building height, T_{min} increases by 1.3 °C for every
16 0.5 increase in the *GnPR*.

17 A comprehensive microclimate optimization framework for urban design in cold
18 regions in China was developed. The building height for a block should be regulated
19 to avoid excessive differences in the building height. For the optimization of both the
20 wind and thermal environment, the *BDG* had better not exceed 30%, and the *HBDG*
21 should be in the range of 3-5 for block unit (in Harbin is 400 m × 400 m). In addition,
22 the proportion of open space in the block should be maximized on the premise of
23 meeting the *BDG* and *HBDG* index.

1

2 **Acknowledgement**

3 This study was supported by the “Heilongjiang Province Philosophy and Social
4 Science Research Planning Project” (18SHB070).

5 **References**

- 6 [1] D. Xu, D. Zhou, et al. Field measurement study on the impacts of urban spatial indicators
7 on urban climate in a Chinese basin and static-wind city, Building and Environment. 147
8 (2019). <https://doi.org/10.1016/j.buildenv.2018.10.042>.
- 9 [2] Y.C. Sin, K.C. Chi. Development of artificial neural network models for predicting
10 thermal comfort evaluation in urban parks in summer and winter, Building and
11 Environment. 164 (2019). <https://doi.org/10.1016/j.buildenv.2019.106364>.
- 12 [3] L. Parreira M. Gäal, C.C. Pezzuto, et al. Urban geometry and the microclimate of street
13 canyons in tropical climate, Building and Environment. 159 (2020).
14 <https://doi.org/10.1016/j.buildenv.2019.106547>.
- 15 [4] M. Huang, P. Cui, X. He. Study of the Cooling Effects of Urban Green Space in Harbin
16 in Terms of Reducing the Heat Island Effect, Sustainability. 10 (1101) (2018).
17 <https://doi.org/10.3390/su10041101>.
- 18 [5] Y. Wang, et al. City-scale morphological influence on diurnal urban air temperature,
19 Building and Environment. 169 (2020). <https://doi.org/10.1016/j.buildenv.2019.106527>.
- 20 [6] S.K. Jusuf, N.H. Wong, Z.Y. Wong, et al. Transformation of industrial planning in
21 Singapore: Study on the micro-climatic condition of different industrial estates. Building
22 and Environment. 80 (2014) 48-60. <https://doi.org/10.1016/j.buildenv.2014.05.015>.
- 23 [7] H. Yan, S. Fan, C. Guo, et al. Assessing the effects of landscape design parameters on

- 1 intra-urban air temperature variability: the case of Beijing, China. Building and
2 environment. 76 (2014) 44-53. <https://doi.org/10.1016/j.buildenv.2014.03.007>.
- 3 [8] T. Yokobori, S Ohta. Effect of land cover on air temperatures involved in the
4 development of an intra-urban heat island. Climate Research. 39 (1) (2009) 61-73.
5 <https://doi.org/10.3354/cr00800>.
- 6 [9] Z.W. Yang, Y.B. Chen, et al. Application of building geometry indexes to assess the
7 correlation between buildings and air temperature, Building and Environment, 167
8 (2020). <https://doi.org/10.1016/j.buildenv.2019.106477>.
- 9 [10] C.P. Miao, S. Yu, et al. Review of methods used to estimate the sky view factor in urban
10 street canyons, Building and Environment. 168 (2020).
11 <https://doi.org/10.1016/j.buildenv.2019.106497>.
- 12 [11] C. Yuan, A.S. Adelia, et al. Mitigating intensity of urban heat island by better
13 understanding on urban morphology and anthropogenic heat dispersion, Building and
14 Environment. 10 (2020). <https://doi.org/10.1016/j.buildenv.2020.106876>.
- 15 [12] A. Aflaki, M. Mirnezhad, et al. Urban heat island mitigation strategies: A state-of-the-art
16 review on Kuala Lumpur, Singapore and Hong Kong, Cities. 62 (2017).
17 <https://doi.org/10.1016/j.cities.2016.09.003>.
- 18 [13] C.J. Zhao, et al. Urban planning indicators, morphology and climate indicators: A case
19 study for a north-south transect of Beijing China, Building and Environment. 5 (46)
20 (2011) 1174-1183. <https://doi.org/10.1016/j.buildenv.2010.12.009>.
- 21 [14] P.K. Cheung, C.Y. Jim. Effects of urban and landscape elements on air temperature in a
22 high-density subtropical city, Building and Environment. 164 (2019).
23 <https://doi.org/10.1016/j.buildenv.2019.106362>.
- 24 [15] Y.J. Yang, E. Gatto, et al. The “plant evaluation model” for the assessment of the impact

- 1 of vegetation on outdoor microclimate in the urban environment, Building and
2 Environment. 159 (2019). <https://doi.org/10.1016/j.buildenv.2019.05.029>.
- 3 [16] E. Krüger, B. Givoni. Outdoor measurements and temperature comparisons of seven
4 monitoring stations: Preliminary studies in Curitiba, Brazil. Building and environment.
5 42 (4) (2007), 1685-1698. <https://doi.org/10.1016/j.buildenv.2006.02.019>.
- 6 [17] S.S. Tong, N.H. Wong, et al. Study on correlation between air temperature and urban
7 morphology parameters in built environment in northern China, Building and
8 Environment. 127 (2018) 239-249. <https://doi.org/10.1016/j.buildenv.2017.11.013>.
- 9 [18] B. Gadhvi, V. Savsani, V. Patel. Multi-Objective Optimization of Vehicle Passive
10 Suspension System Using NSGA-II, SPEA2 and PESA-II, Procedia Technology. 23
11 (2016). <https://doi.org/10.1016/j.protcy.2016.03.038>.
- 12 [19] J.D. Schaffer. Multiple Objective Optimization with Vector Evaluated Genetic
13 Algorithms, Proceedings of the 1st International Conference on Genetic Algorithms,
14 Pittsburgh, PA, USA, July 1985. Lawrence Erlbaum Associates Publishers, Hillsdale,
15 1985.
- 16 [20] D.E. Goldber. Genetic Algorithms in Search, Optimization and Machine Learning.
17 Addison-Wesley Pub. Co, 1989.
- 18 [21] Inês Costa-Carrapiço, Rokia Raslan, Javier Neila González. A systematic review of
19 genetic algorithm-based multi-objective optimisation for building retrofitting strategies
20 towards energy efficiency, Energy and Buildings. 210 (2020).
21 <https://doi.org/10.1016/j.enbuild.2019.109690>.
- 22 [22] X. Chen, P.N. Xue, L. Liu, L.X .Gao, J. Liu. Outdoor thermal comfort and adaptation in
23 severe cold area: A longitudinal survey in Harbin, China, Building and Environment. 143
24 (2018) 548-560. <https://doi.org/10.1016/j.buildenv.2018.07.041>.

- 1 [23] S.S. Tong, N.H. Wong, et al. Impact of urban morphology on microclimate and thermal
2 comfort in northern China, Solar Energy. 155 (2017) 212-223.
3 <https://doi.org/10.1016/j.solener.2017.06.027>.
- 4 [24] L. Liu, Y.Y. Lin, et al. Analysis of local-scale urban heat island characteristics using an
5 integrated method of mobile measurement and GIS-based spatial interpolation, Building
6 and Environment. 117 (2017). <https://doi.org/10.1016/j.buildenv.2017.03.013>.
- 7 [25] L. Yang, K. Lyu, H.L. Li, Y. Liu. Building climate zoning in China using supervised
8 classification-based machine learning, Building and Environment. 171 (2020).
9 <https://doi.org/10.1016/j.buildenv.2020.106663>.
- 10 [26] D. Fröhlich, M. Gangwisch, A. Matzarakis. Effect of radiation and wind on thermal
11 comfort in urban environments - Application of the RayMan and SkyHelios model,
12 Urban Climate. 27 (2019) 1-7. <https://doi.org/10.1016/j.uclim.2018.10.006>.
- 13 [27] H. Jin, P. Cui, N.H. Wong, M. Ignatius. Assessing the Effects of Urban Morphology
14 Parameters on Microclimate in Singapore to Control the Urban Heat Island Effect,
15 Sustainability. 10 (206) (2018). <https://doi.org/10.3390/su10010206>.
- 16 [28] Grasshopper - algorithmic modeling for Rhino, <https://www.grasshopper3d.com>, (2020).
- 17 [29] T.Y Xin, C. Qiao, H. Wang, H. Jin. Influence of outdoor thermal environment on
18 clothing and activity of tourists and local people in a severely cold climate city, Building
19 and Environment. 173 (15) (2020). <https://doi.org/10.1016/j.buildenv.2020.106757>.
- 20 [30] B. David, D.S. Garcia, et al. Optimization of energy-saving with adaptive set point
21 temperatures by calculating the prevailing mean outdoor air temperature. Building and
22 Environment. 170 (2020). <https://doi.org/10.1016/j.buildenv.2019.106612>.

Table 1. Technical characteristics of measurement instruments

Temperature/RH	WBGT-2006
	Global temperature (T_g) -40°C to 70°C, ± 0.18°C
	HOBO UX100-014M
	Temperature range/accuracy -40 °C to 70 °C, ±0.2 °C
	RH measurement range/accuracy 0%-100%, ± 2.5%
Wind speed/ direction	NK4500 weather station
	Wind direction range 2-Axis ultrasonic wind sensor
	Wind speed range/accuracy 0-45 m/s (0-100 mph) ±1.1m/s(2.4mph)
Sky view factor (SVF)	Canon 5D2 camera with fish eye lens

Table 2. Selected days for model development and validation

	30 days for model development	5 days for model validation	
Dec 2017	10, 18,20	Dec 2017	17
Jan 2018	11, 13, 15, 25	Feb 2018	15
Feb 2018	2, 8, 9	Apr 2018	14
Mar 2018	5, 7, 8	Jun 2018	18
Apr 2018	2, 5, 6	Aug 2018	20
May 2018	20, 26, 27		
Jun 2018	22, 23, 25, 26		
Jul 2018	5, 8, 16		
Aug 2018	5, 6, 10, 18		

Table 3 Description of measuring points (100m)

No	SVF		GnPR		BDG	HBDG	PAVE (%)	WALL (m ²)	Description of measurement points
	Winter	Summer	Winter	Summer	(%)	(m)			
1	0.58	0.52	0.34	0.55	15	2.7	30	3035.34	Broad street with avenue tree, multi-storey buildings
2	0.50	0.39	0.198	0.32	35	6.3	33	7082.46	Broad street with avenue tree, multi-storey buildings
3	0.80	0.40	0.427	0.69	21	7.56	10	8498.952	High-rise buildings, shade tree
4	0.61	0.35	0.341	0.55	12	2.52	33	2832.984	Broad street with avenue tree, multi-storey buildings
5	0.78	0.69	0.372	0.6	0	0	94	0	Open area with trees and lawn
6	0.49	0.36	0.136	0.22	20	3.6	56	4047.12	Broad street with avenue tree, multi-storey buildings
7	0.52	0.43	0.341	0.55	35	17.5	10	19673.5	High-rise buildings, shade tree
8	0.65	0.60	0.148	0.24	12	1.44	64	1618.848	Open area with few trees
9	0.92	0.48	0.18	0.30	28	4.2	42	4721.64	Pedestrian street with avenue tree, multi-storey buildings
10	0.40	0.36	0.09	0.15	50	7.5	35	8431.5	Pedestrian street with avenue tree,

										multi-storey buildings
11	0.32	0.20	0.13	0.18	40	6	42	6745.2	Pedestrian street with avenue tree, high-rise buildings buildings	
12	0.26	0.24	0.074	0.12	36	5.4	52	6070.68	Pedestrian street with avenue tree, high-rise buildings buildings	
13	0.22	0.19	0.48	0.77	18	0.54	5	607.064	Park's perimeter road, tree cover	
14	0.37	0.09	0.496	0.80	8	0.24	12	269.808	Park's perimeter road, tree cover	
15	0.31	0.31	0.078	0.12	77	27.72	11	31162.824	High-rise buildings, without tree	
16	0.66	0.66	0.31	0.5	68	28.56	17	32107.152	High-rise buildings, without tree	
17	0.62	0.62	0.17	0.25	30	5.4	45	6070.68	Enclosed building without tree	
18	0.20	0.18	0.111	0.18	42	10.08	40	11331.936	Broad street without tree, multi-storey buildings	
19	0.55	0.45	0.12	0.20	46	8.28	34	9308.376	Broad street with avenue tree, multi-storey buildings	
20	0.72	0.72	0.49	0.8	7	0.42	85	472.164	Open area with few tree	
21	0.58	0.34	0.496	0.8	36	6.48	56	7284.816	Broad street with avenue tree, High-rise buildings	
22	0.50	0.50	0.31	0.5	48	8.64	47	9713.088	Broad street with avenue tree, multi-storey buildings	
23	0.53	0.42	0.111	0.18	59	10.62	25	11939.004	Broad street without tree, multi-storey buildings	
24	0.42	0.37	0.191	0.26	15	2.7	59	3035.34	Broad street with avenue tree, High-rise buildings	
25	0.44	0.33	0.094	0.12	32	5.76	56	6475.392	Enclosed multi-storey building without tree	
26	0.41	0.37	0.09	0.14	38	4.56	48	4104	Open area without trees	
27	0.40	0.40	0.22	0.34	21	3.78	45	3024	Open area with few trees	

Table 4. Correlation analysis of urban morphology parameters and temperature in different buffer radii ($P < 0.05$)

R^2	20m		50m		100m		150m		200m	
	T>0 °C	T<0 °C								
T_{min}	0.58	0.66	0.77	0.77	0.95	0.79	0.78	0.82	0.65	0.71
T_{avg}	0.41	0.76	0.89	0.90	0.92	0.90	0.83	0.85	0.67	0.73
T_{max}	0.33	0.81	0.63	0.81	0.90	0.88	0.81	0.81	0.78	0.79

Table 5. Correlation analysis of urban morphology parameters and temperature in 100 m radius

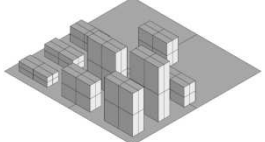
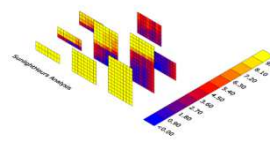
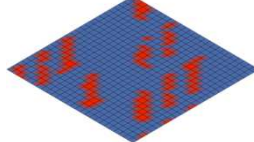
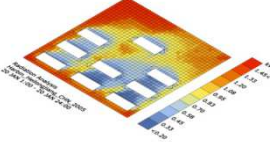
<i>Ref T</i>	<i>T_{min}</i>			<i>T_{avg}</i>			<i>T_{max}</i>				
	>0 °C	<0 °C	B	Sig.	P	B	Sig.	P	B	Sig.	P
<i>Ref T</i>	0.736/0.837	0.0/0.0	0.90/0.93	0.99/0.99	0.0/0.0	0.71/0.65	0.72/0.73	0.0/0.0	0.61/0.79		
<i>Solar</i>	--	--	--	4.8E-05/5.7E-05	0.0/0.0	0.34/0.21	0.002/0.093	0.0/0.0	0.11/0.25		
<i>RH</i>	0.001/0.002	0.7/0.2	0.02/0.02	-0.02/0.002	0.0/0.4	-0.07/0.21	0.001/0.001	0.09/0.06	0.1/0.06		
<i>WIND</i>	-0.122/-0.09	0.0/0.0	-0.21/-0.17	-0.18/-0.021	0.0/0.0	-0.22/0.12	-0.33/-0.13	0.0/0.2	0.28/0.33		
<i>PAVE</i>	0.02/0.004	0.0/0.0	0.31/0.08	0.01/0.007	0.0/0.0	0.33/0.07	0.015/0.001	0.0/0.0	0.21/0.07		
<i>GnPR</i>	-0.31/-0.03	0.0/0.0	-0.21/-0.07	-0.04/0.06	0.0/0.0	-0.29/0.11	0.007/0.09	0.11/0.56	-0.28/-0.41		
<i>HBDG</i>	-0.04/0.992	0.0/0.0	-0.21/0.38	-0.02/0.09	0.0/0.0	-0.09/0.06	-0.026/0.016	0.0/0.0	-0.07/0.08		
<i>WALL</i>	2.2E-06/5.1E-06	0.0/0.0	0.1/0.6	2.1E-05/2.3E-05	0.0/0.0	0.32/0.21	2.2E-05/6.7E-06	0.0/0.0	0.11/0.28		
<i>SVF</i>	-0.21/0.35	0.1/0.5	-0.3/0.5	0.81/1.32	0.0/0.0	0.07/0.12	1.43/1.41	0.0/0.0	0.31/0.39		
Constant		3.021/3.261			3.177/3.434				1.542/1.228		
<i>F</i>		2907.12/2194.45			2280.11/2243.54				2242.45/2113.33		
<i>R²</i>		0.96/0.90			0.97/0.95				0.96/0.91		
<i>Std. Error</i>		0.24/0.31			0.21/ 0.23				0.25/0.34		

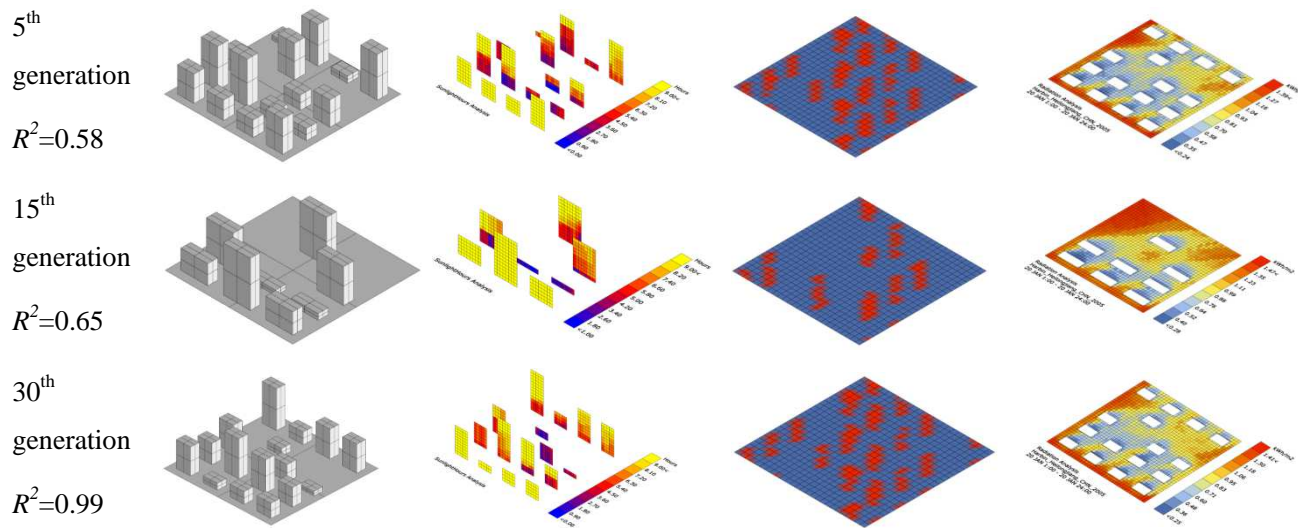
Table 6. Correlation between air temperature and urban morphology parameters

<i>Ref T > 0°C</i>	$T_{min} = 3.021 + 0.736 \text{Ref } T_{min} - 0.122WIND + 0.02PAVE - 0.31GnPR - 0.04HBDG + 2.2 \times 10^{-6}WALL$ ($R^2 = 0.96, F = 2907.12, Std. Error = 0.24, Sig. 0.00$)
	$T_{avg} = 3.177 + 0.997\text{Ref } T_{avg} - 0.02RH - 0.18WIND + 4.799 \times 10^{-5}SOLAR + 0.01PAVE - 0.04GnPR - 0.02HBDG + 2.121 \times 10^{-5}WALL + 0.81SVF$ ($R^2 = 0.97, F = 2280.11, Std. Error = 0.21, Sig. 0.00$)
	$T_{max} = 1.542 + 0.72\text{Ref } T_{max} + 0.002SOLAR + 0.01PAVE - 0.33WIND - 0.026HBDG + 2.2 \times 10^{-5}WALL + 1.43SVF$ ($R^2 = 0.96, F = 2242.45, Std. Error = 0.25, Sig. 0.00$)
<i>Ref T < 0°C</i>	$T_{min} = 3.261 + 0.837 \text{Ref } T_{min} - 0.09WIND + 0.004PAVE - 0.03GnPR + 0.992 HBDG + 5.121 \times 10^{-6}WALL$ ($R^2 = 0.90, F = 2194.45, Std. Error = 0.31, Sig. 0.00$)
	$T_{avg} = 3.434 + 0.991\text{Ref } T_{avg} - 0.02RH + 5.712 \times 10^{-5}SOLAR + 0.007PAVE + 0.06GnPR + 0.095HBDG + 2.33 \times 10^{-5}WALL + 1.32SVF$ ($R^2 = 0.95, F = 2243.54, Std. Error = 0.23, Sig. 0.00$)
	$T_{max} = 1.228 + 0.73\text{Ref } T_{max} + 0.093SOLAR + 0.001PAVE + 0.016HBDG + 6.73 \times 10^{-6}WALL + 1.41SVF$ ($R^2 = 0.91, F = 2113.33, Std. Error = 0.34, Sig. 0.00$)

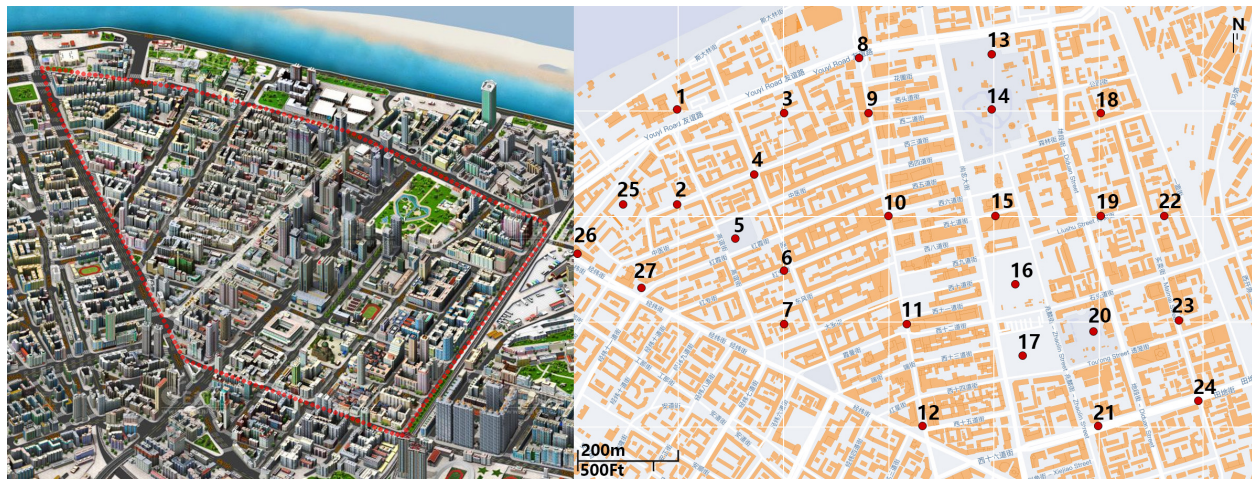
Table 7. The calculation results of the optimal solution sets of different generation

(The image in the table is one of the optimal solution set in this generation)

	The optimization layout	Sunshine duration calculate	Wind pressure differential calculate	Temperature calculate
1 st generation $R^2=0.43$				

**Table 8.** Simplify model parameter Settings

Model		1	2
Morphological parameter	Building levels (3 m per storey)	1-40	1-40
	Pavement width (W)	15m/25m/35m/45m	35m
	Greenery strips width	5m	5m
	GnPR	1.5	0.5/1/1.5/2/2.5
Weather parameter		Summer	Winter
	SOLAR(W/m ²)	811	454
	Ref T _{avg} (°)	22.8	-8.6
	Ref T _{max} (°)	29.5	-3.3
	Ref T _{min} (°)	22.1	-15.6





NK4500 weather station

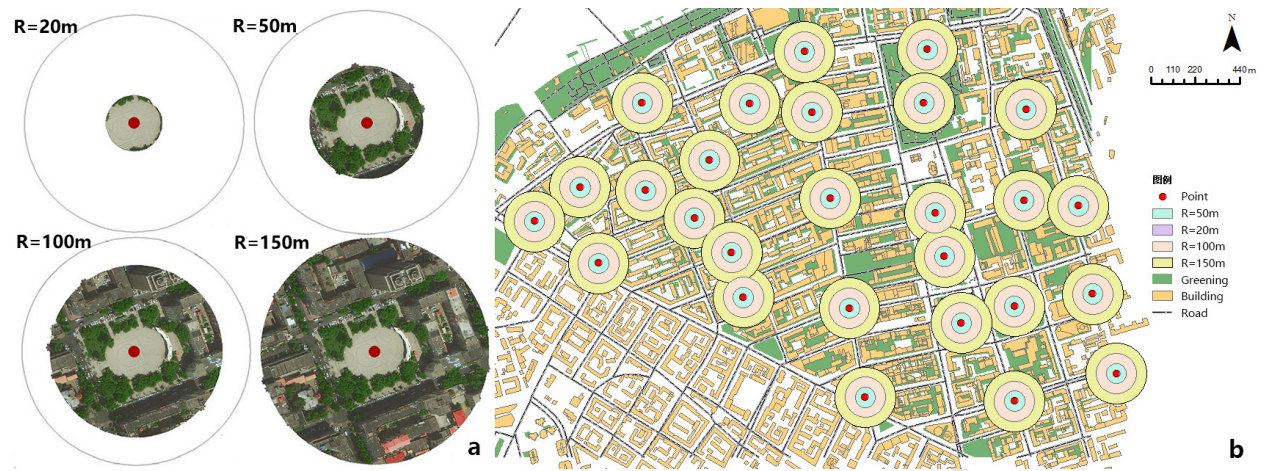
Black-bulb thermometer

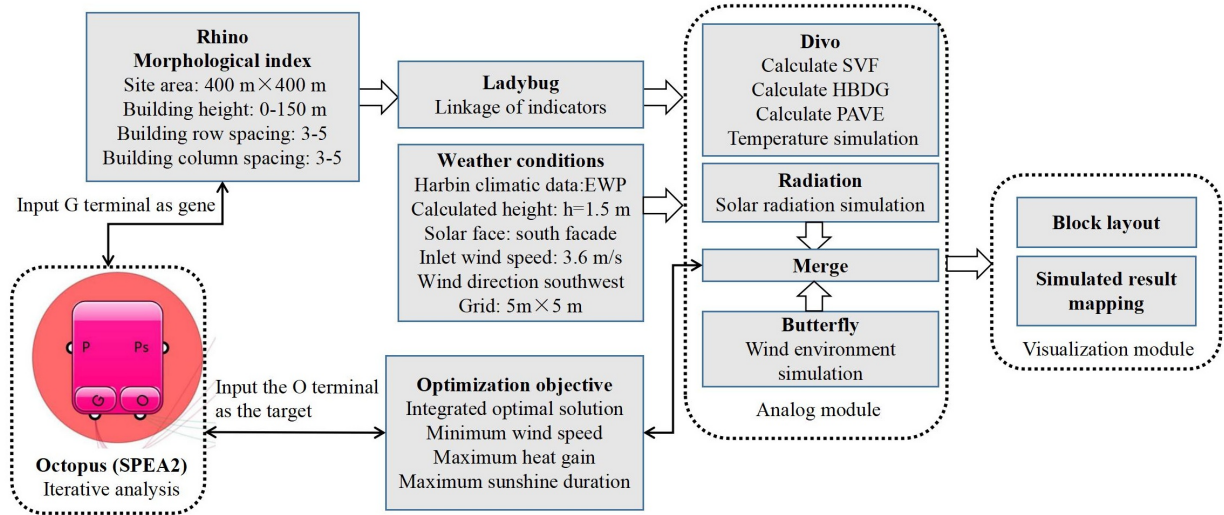
HOBO UX100-014M

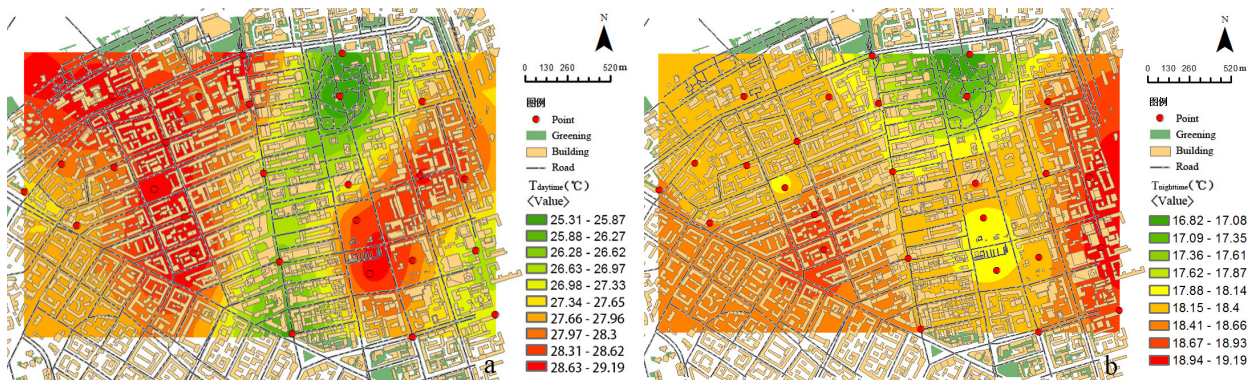
Aluminium foil

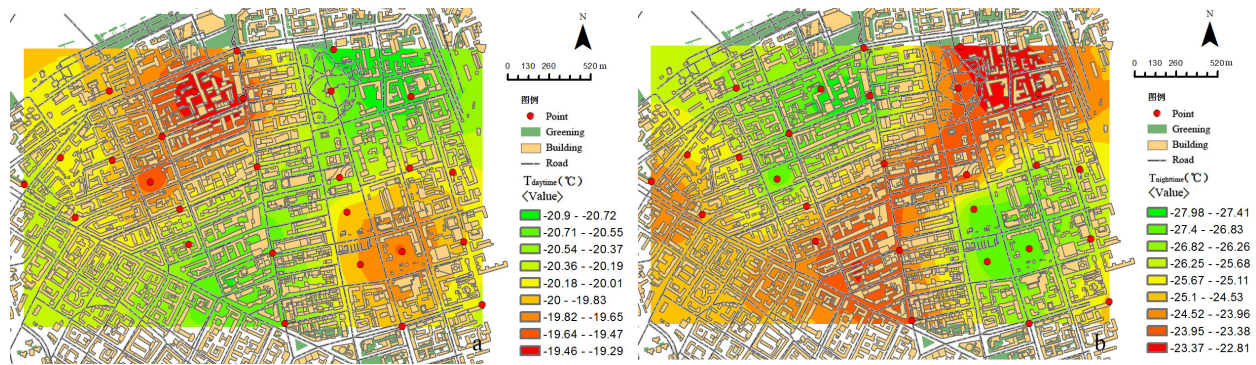
Tripod

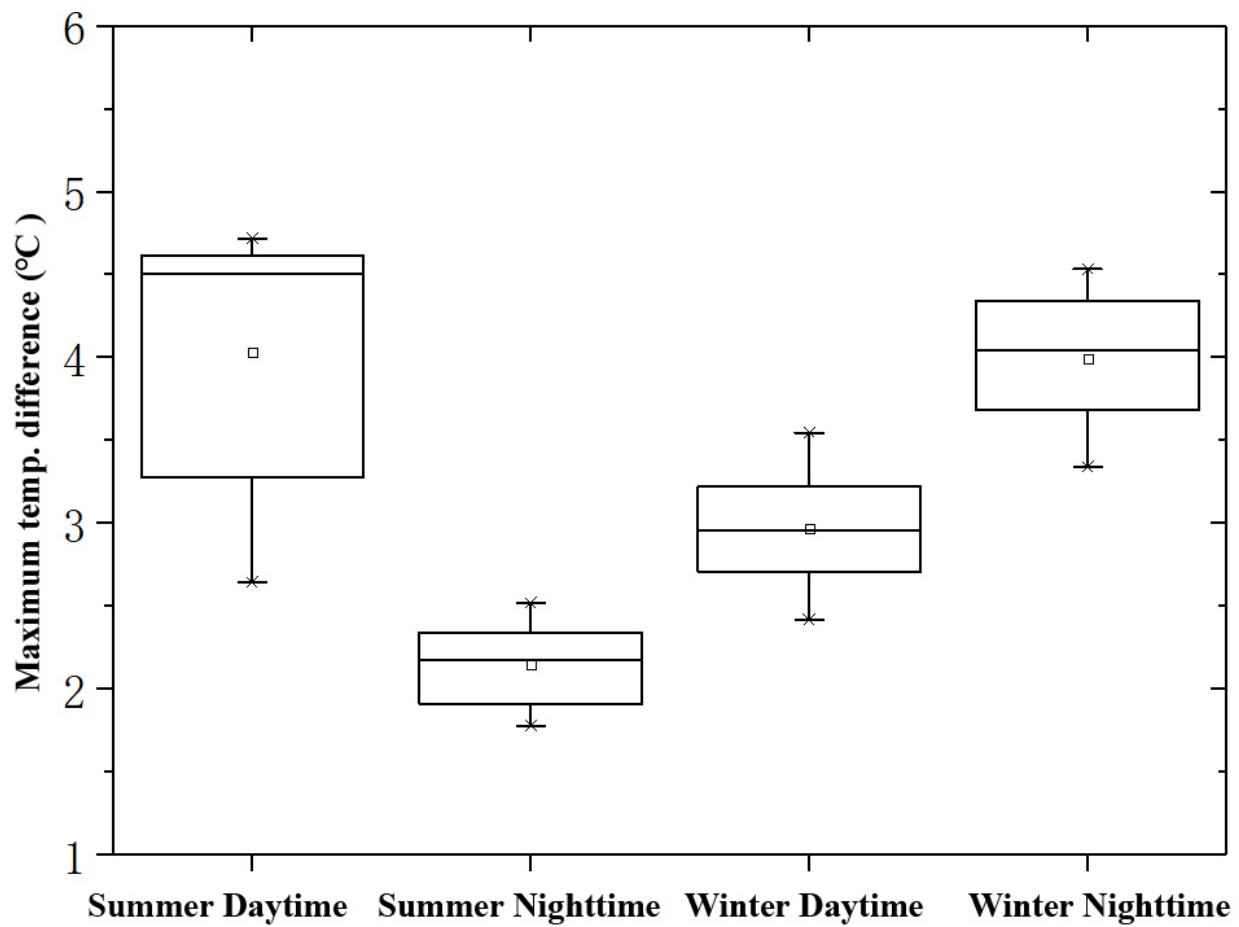


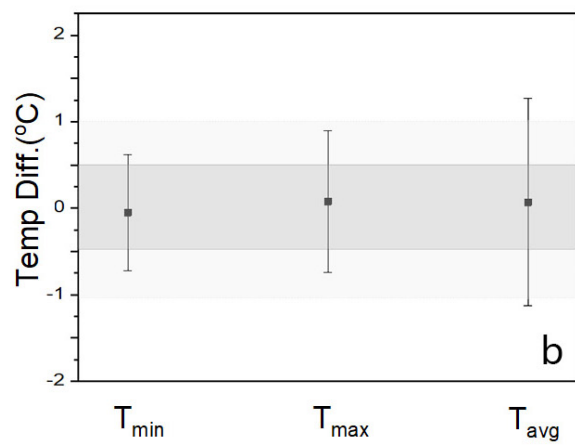
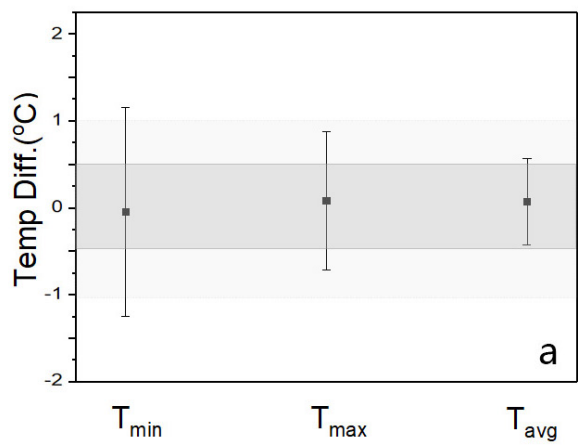


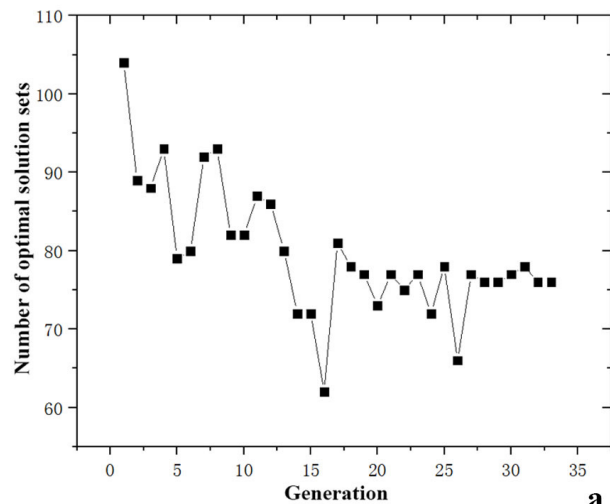
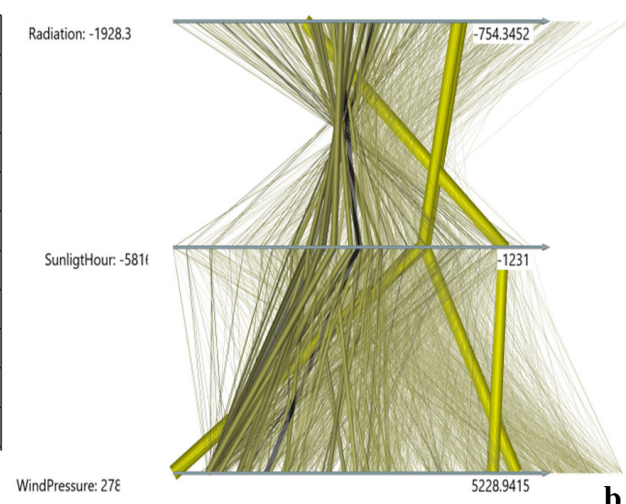
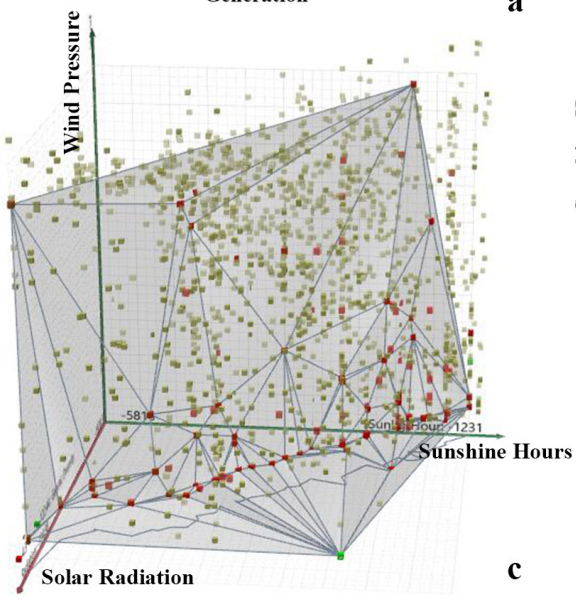
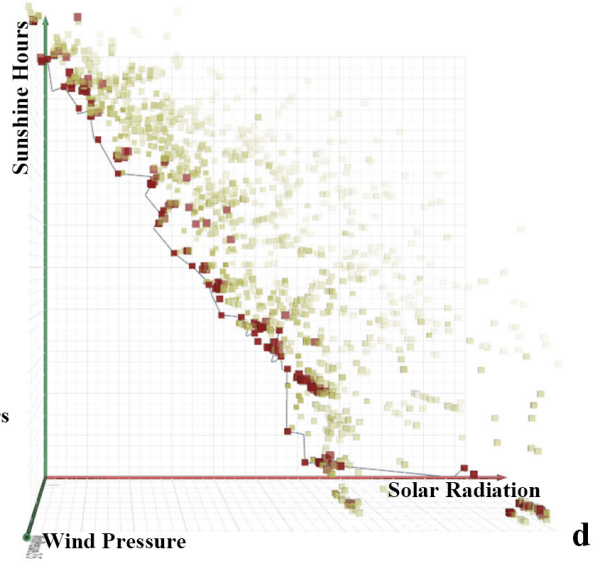


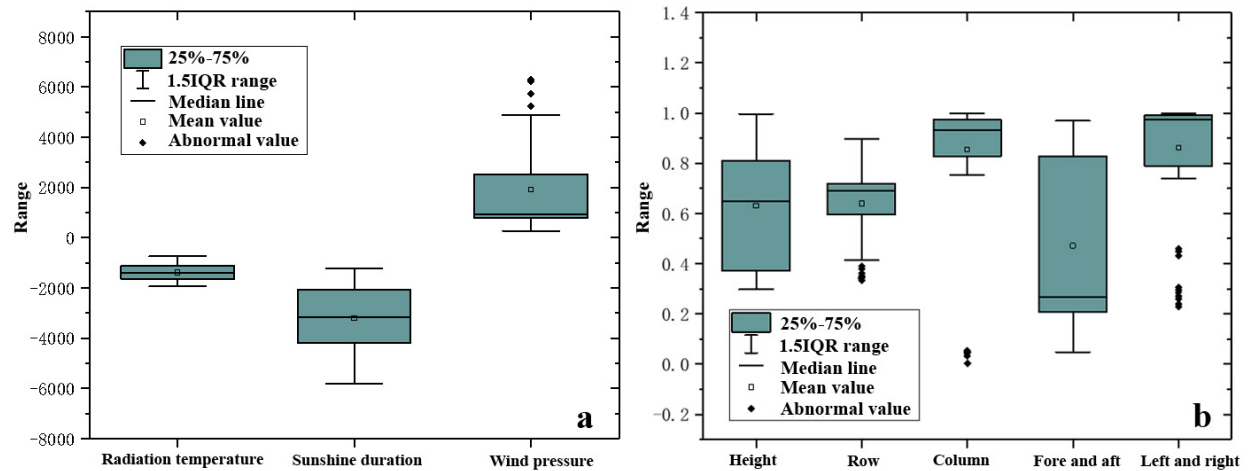


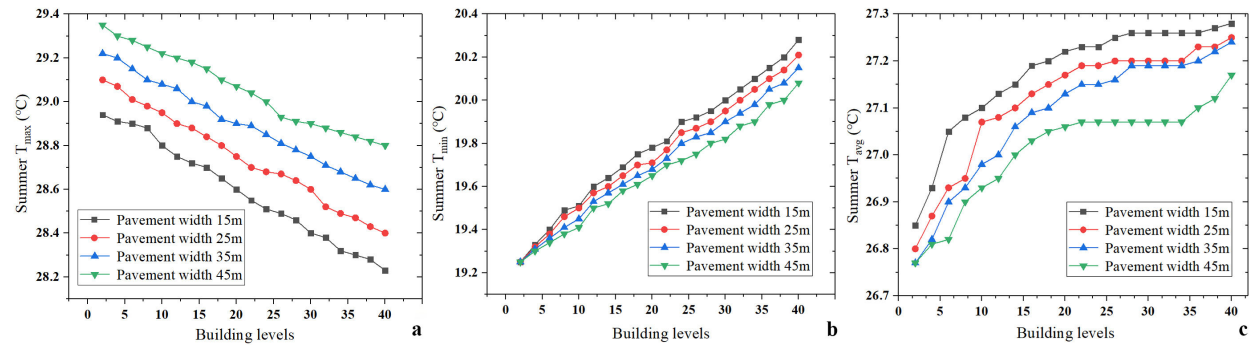


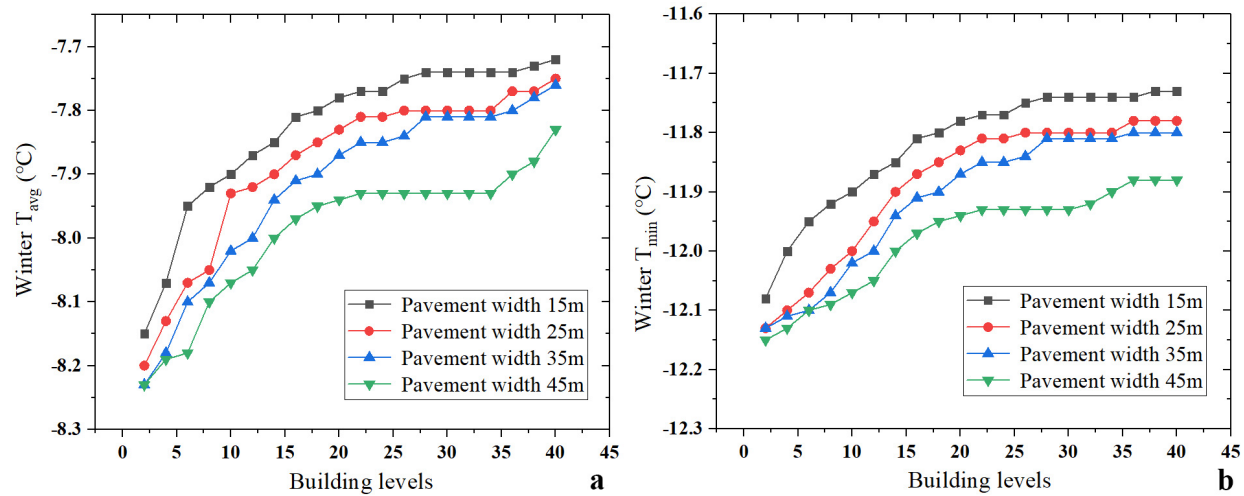


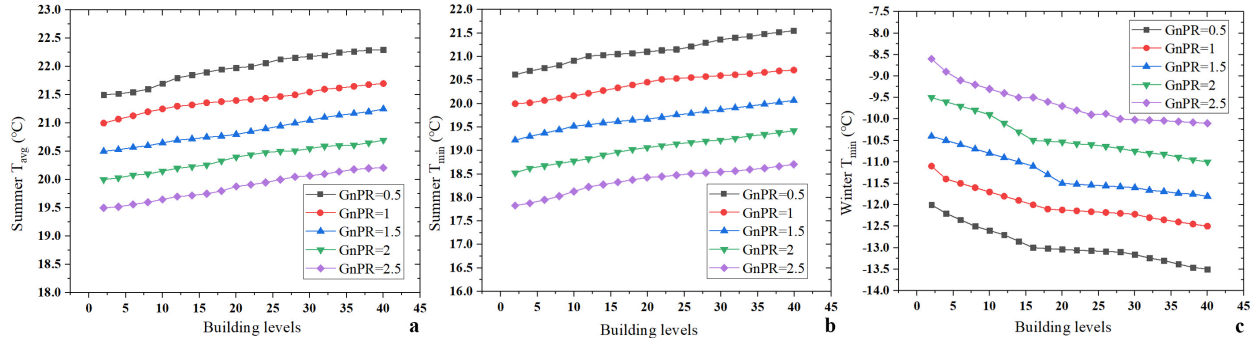


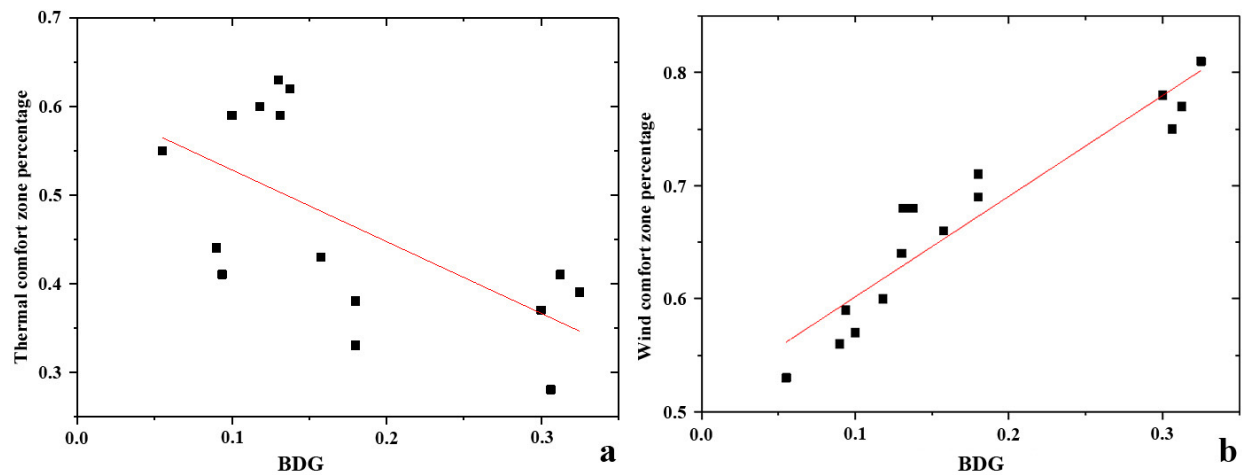
**a****b****c****d**

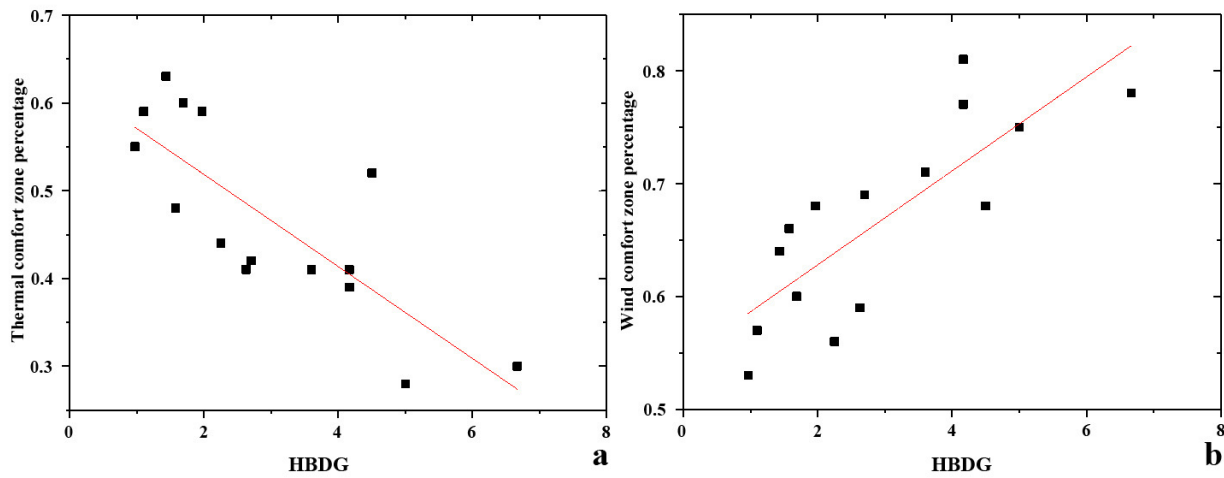












Highlights

1. Empirical models were proposed to predict the spatial variations of air temperature.
2. Parametric study was done to quantify the impact of urban morphology on temperature.
3. Multi-objective optimization framework was proposed to optimize block microclimate.
4. The SPEA-2 algorithm is applied to find the Pareto optimal solutions.
5. Series of design-based recommendations were presented for early urban design stage.

Declaration of interests

The authors declare that they have no known competing financial interests or personal relationships that could have appeared to influence the work reported in this paper.

The authors declare the following financial interests/personal relationships which may be considered as potential competing interests:

